Experimental Investigation on the dissimilar laser weld joints between Inconel 625 Superalloy and AISI 430 Ferritic Stainless Steel

M. Emadi [1], H. Mostaan [2,*] , M. Rafiei [1]

[1] *Advanced Materials Research Center, Department of Materials Engineering, Najafabad Branch, Islamic Azad University, Najafabad, Iran*
[2] *Faculty of Engineering, Department of Materials and Metallurgical Engineering, Arak University, Arak 38156-8-8349, Iran*

ARTICLE INFO

Article history:

Received 17 January 2020
Accepted 15 April 2020
Available online 15 September 2020

Keywords:

Inconel 625
430 ferritic stainless steel
Optimization
Laser welding
Dissimilar joint

ABSTRACT

Mechanical properties optimization of weldment such as tensile strength, microhardness and impact toughness are of prime importance in welding technology. The main aim of this research is to investigate the microstructural evolutions and also optimization of tensile strength in dissimilar laser welding between Inconel 625 superalloy and AISI 430 ferritic stainless steel. It was found from the microhardness measurements that the hardness is increased form AISI 430 base metal toward Inconel 625 superalloy. This can be attributed to the inherent higher hardness of Inconel 625 and formation of very fine structure and also fine precipitations in the weld metal which are distributed uniformly. Formation of very fine structure and precipitations is due to the rapid cooling rate of the weld metal during laser welding process. Design of experiment based on the response surface method was used in order to optimize the tensile strength of the weld joints. Three process parameters i. e. pulse duration, lamping current and also travel speed were chosen as the main parameters which are considerably affecting the tensile strength of the weld joint. It was found that the lamping current has a higher impact on the tensile strength of the weld joints.

1-Introduction

Dissimilar welding between various materials and alloys are extensively used in many industrial applications. A defect free weld joint is one of the main issues in the welding processes which are used in oil, petrochemical and also power generation applications. Besides chemical composition of base metal and filler metal, welding process parameters play a major role in microstructural features and are effective factors which specify corrosion resistance, mechanical properties and weldability of metals. In many cases, joining of nickel based alloys to stainless steels at elevated temperatures and corrosive environments is inevitable. On the other hand, replacing of nickel based alloys by stainless steel is necessary to reduce cost [1].

Inconel 625 is one of the well-known nickel based superalloys which is strengthened by adding chromium and niobium alloying elements and formation a solid solution. This alloy has a good weldability [2]. Ferritic stainless steels are soft magnetic materials and have excellent corrosion resistance. Theses alloys are inherently don't considered as weldable metals but owing their excellent soft magnetic properties and very good

* Corresponding author:
E-mail address: H-mostaan@araku.ac.ir

machinability are extensively used in solenoid valves in chemical environments [3].

Laser welding is an appropriate joining process of high temperature materials such as nickel based alloys. Low heat input, high power density and high travel speed are the main advantageous of laser welding process [3]. The costs are still the biggest disadvantage of this innovative process. In addition, Weldment position must be accurate; it should be controlled in the focusing range of laser beam. Moreover, the weldability of high reflectivity & high-thermal conductivity material would be changed by laser, such as aluminum, copper and their alloy etc. Weld bead geometry, mechanical behavior and welding induced distortion are the most important criteria which determine the weld joint quality. The heat input to the materials caused by welding process can undesirably change the above-mentioned features. The welding process parameters affect heat input and consequently play an important role in determining the performance of welded joints [4,5]. Therefore, choosing of the proper welding process parameters in order to attain an improved weld quality is always a challenge for welding engineers. Design of experiment is a suitable method which is used in various manufacturing industries in order to improve the quality of productions [5-8]. Ramkumar et al. studied gas tungsten arc welded joint between Inconel 718 and AISI 430 ferritic stainless steel. The welding was carried out by ER2553 and ERNiCrMo-4 filler metals. The obtained results showed that a homogenous weld metal is formed by welding with these two filler metals and grain coarsening and also formation of Nb-riched phases are occurred in the heat affected zones of 430 ferritic stainless steel and Inconel 718, respectively. Laves and sigma phases were not observed in the ERNiCRMo-4 weld metal. Moreover, no solidification or liquation cracking was observed owing the presence of niobium and molybdenum elements. The microhardness measurements showed that the hardness of ER2553 weld metal is higher than that of ERNiCrMo-4 weld metal due to the presence of skeletal delta ferrite. In addition, the hardness of ERNiCrMo-4 is higher than that of AISI 430 base metal. It was also reported that in both weld metal no crack, microfissure and lamination are formed during bending test [7].

To the author's knowledge, no research was found in the literature on the dissimilar welding between Inconel 625 and AISI 430 stainless steel. Hence, the main aim of this research is to investigate the microstructural evolutions during laser welding of Inconel 625 and AISI 430 stainless steel base metals. Also, an attempt was done on the optimization of laser welding parameters in order to obtain the maximum tensile strength of the weld joints. The authors believe that the results of this study would help with exploiting full advantages of these alloys.

2- Materials and experimental procedures

2-1- Base metals and experiments

The used base metals in this study were Inconel 625 and AISI 430 ferritic stainless steel with thickness of 0.8 mm. the chemical compositions of the alloys were analyzed by optical emission spectroscopy (OES) method and the results are shown in Table 1. The lap joint configuration was chosen for joining of these two base metals and a fixture was used for this purpose as shown in Fig. 1. The selected parameters and their levels are listed in Table 2.

Table 1. Chemical compositions of the base metals.

	Weight percent of the elements										
Base metals	***Fe***	***Ni***	***Cr***	***Mo***	***Mn***	***Nb***	***C***	***Si***	***Cu***	***Ti***	
Inconel625	*4.85*	*base*	*21.07*	*8.59*	*trace*	*3.70*	*0.043*	*	*0.03*	*0.27*	***A l-0.16, Co - 0.09, S-0.008, P-0.15, B-0.003***
AISI430	*base*	*0.14*	*17.09*	*0.02*	*0.36*	*0.02*	*0.30*	*0.32*	*0.02*	*0.009*	***S-0.005, P-0.018, B-0.003***

Fig. 1. Experimental set-up for laser welding used in this study.

Table 2. The selected process parameters, symbols and working range.

Parameters	***Unit***	***Symbol***		***Working range***	
			-1	0	1
Lamping current	A	*I*	130	157	185
Travel Speed	mm/s	*V*	5	6.7	8.3
Pulse Duration	ms	T_p	6	7.5	9

The welding process was done normal to the rolling direction of the sheets using a Nd:YAG (IQL-20) laser machine. In order to avoid any weld pool contamination from surrounding atmosphere, Argon inert gas was used as a shielding gas with a flow rate of about 20 l/min. In all cases, the focal length and also pulse frequency were considered 4 mm and 20 Hz, respectively. In order to decrease the systematic errors in experiments, the welding process runs were performed randomly.

In order to investigate the microstructural and metallurgical evolutions, the welded samples with full penetration were chosen and cut from the weld seam cross section. Revealing the microstructure was done in two steps: the first step for etching AISI 430 stainless steel and the second one for etching Inconel 625, Vilella (5 ml HCl, 1 g picric acid, and 100 ml ethanol) and Kalling (5 g CuCl2, 100 ml HCl, 100 ml ethanol) reagents were used for macro etching of AISI 430 stainless steel and Inconel 625, respectively. An optical microscope was used in order to metallographic observations.

Microstructure of the welded area and the fracture surfaces were analyzed using WEGA TESCAN scanning electron microscope (SEM) equipped with energy dispersive x-ray spectroscopy (EDS) system.

Tensile test specimens were cut from the welded samples using wire cut machine according to Fig. 2 [9].

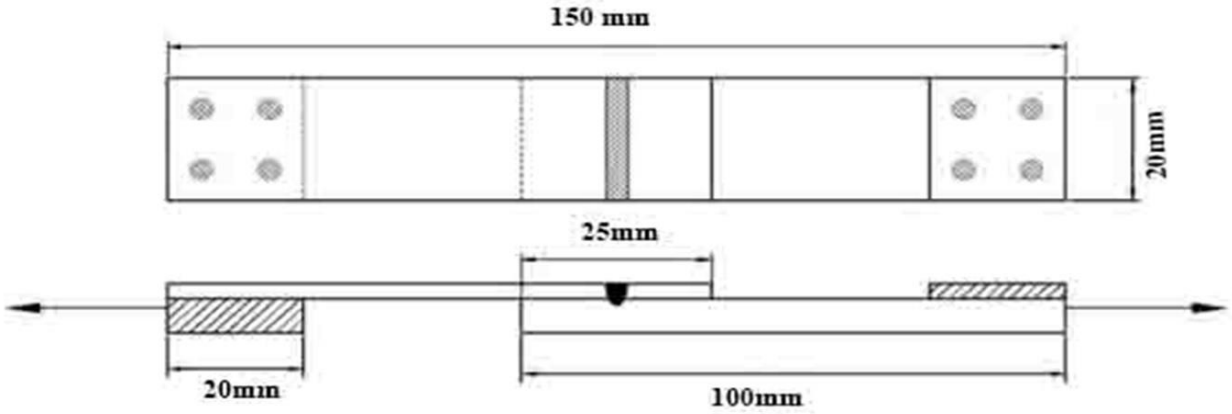

Fig. 2. Dimension of the tensile test specimen [9].

An INSTRON4486 universal tensile test machine was used for tensile test. Figure 3 shows a typical sample of the tensile test specimens.

3-Results and discussions

3-1- Microstructure of the weld metal

The macrostructure of a typical laser welded sample is shown in Fig. 4.

As can be seen, the weld bead profile is acceptable and is free from any crack. Figure 5 shows the optical micrographs of fusion zone microstructure. It can be observed that the microstructure is fully austenitic which is solidified with a dendritic morphology. The microstructures from two different regions of fusion zone are shown in Fig. 6 in which the direction growth of dendrites is different in each grain. In other words, a competitive growth between the grains and solidification boundaries can be revealed. Actually, these boundaries are the interface between packets with aligned dendrites. Toward fusion boundary, the columnar grains and dendrites are observable. However, some equiaxed grains can be seen in this area (See Fig. 7).

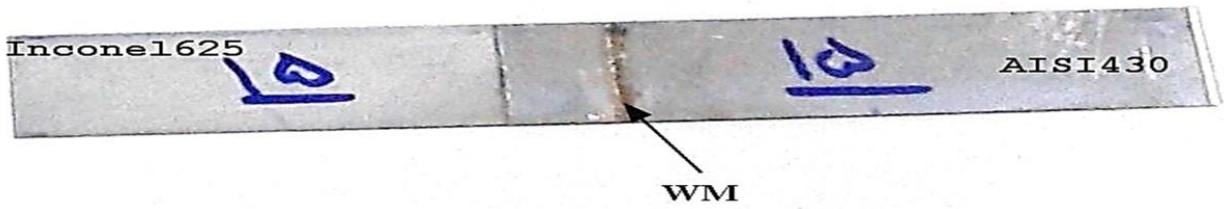

Fig. 3. A typical tensile test specimen of dissimilar laser weld joint.

Fig. 4. Macrostructure of a laser weld joint between Inconel 625 and AISI 430 stainless steel.

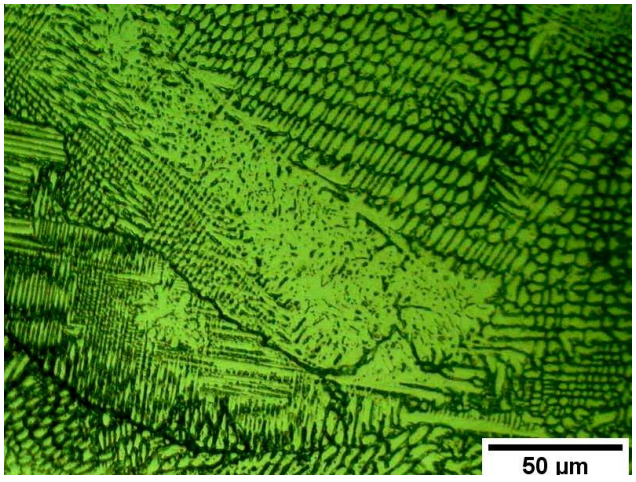

Fig. 5. Optical micrograph of laser welded fusion zone.

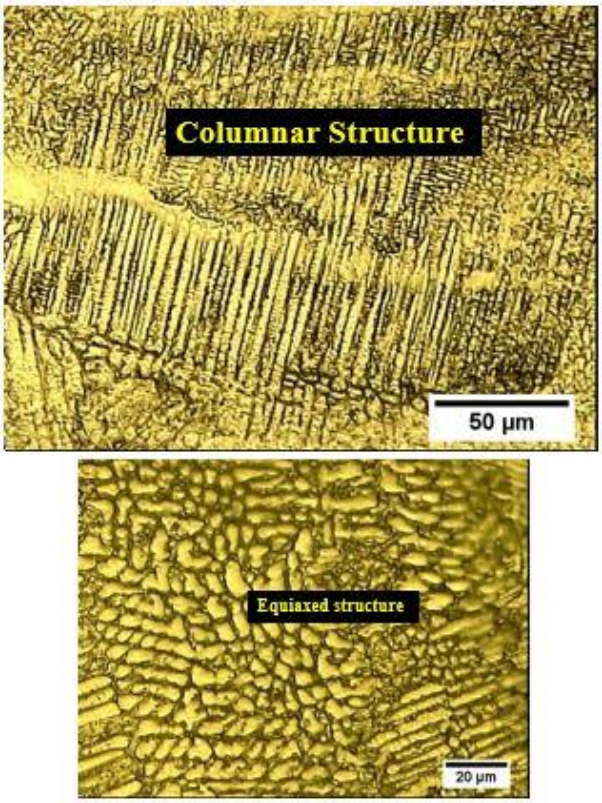

Fig. 6. Optical micrographs of fusion zone showing equiaxed and columnar dendritic structures.

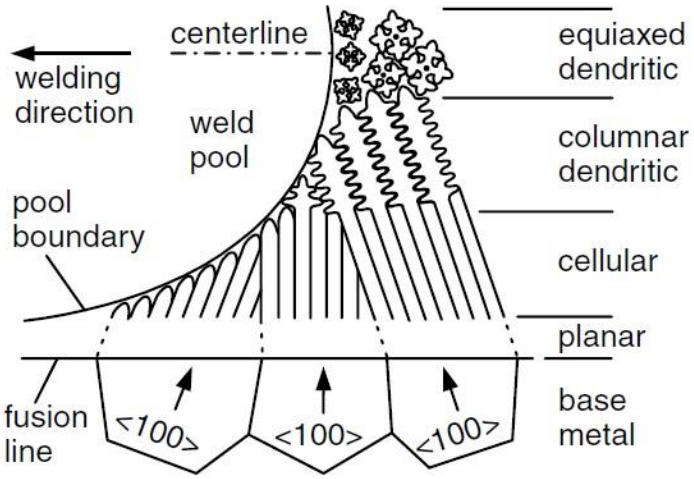

Fig. 7. Variation in solidification mode across fusion zone [14].

It has been shown that the solidification mode is changed in the fusion zone from the fusion line toward center line [10, 11]. Niobium and molybdenum as two major alloying elements in the Inconel 625 are prone to segregate during solidification of the weld metal. Rapid solidification in laser welding process lead to a high undercooling and consequently formation a very fine structure during this process. Difference in undercooling value at the solidification front due to the presence of various alloying elements, especially those with distribution coefficient lower than 1 (such as niobium and molybdenum) lead to formation a columnar dendritic structure and also formation a second phase between these areas. Weld metal microstructure in vicinity of heat affected zones has a columnar dendritic structure so that a composition gradient is created in these areas. On the other hand, accumulated alloying elements recoiled from solidified weld metal in the core of dendritic

arms lead to severe segregation. This is more severe in the laser welding process which has a rapid solidification.

To clarify this, the following equation should be considered:

$$\frac{-mc_0(k-1)}{kD_L} \leq \frac{G}{R} \quad (1)$$

Where G is temperature gradient, D_L denotes to diffusion coefficient in liquid phase, m stands for the slope of liquidus line, k and R are distribution coefficient and solidification rate, respectively.

It has been shown that in a constant temperature gradient, the solidification rate in the center line is maximum, whereas this value is minimum in fusion line. On the other hands, it has been shown that by decrease of G to R ratio from fusion line toward center line the solidification mode is changed from columnar dendritic to equiaxed structure. This is due to the inverse relation between G/R ratio to constitutional undercooling and therefore decrease in G/R value leads to increase in constitutional undercooling and hence formation of an equiaxed structure is favored.

It should be noted that the heat input is also an effective factor on the microstructure. It has been shown that in a constant welding speed, temperature gradient (G) is decreased by increase in heat input and hence the G/R ratio is decreased and constitutional undercooling at the front of solid/liquid interface is increased. In this condition an equiaxed structure is expected to be formed (Fig. 7). So, equiaxed structure is formed in the center line and then columnar dendritic structure is created in vicinity of fusion line [10, 11].

Segregation of alloying elements can be considerably influenced by solidification rate and some theories have been developed in order to make a correlation between microsegregation of alloying elements [10]. Segregation of alloying elements is restricted at high solidification rates such as laser welding process. Restriction of alloying elements-rich solid dendritic or interdendritic liquid can cause a significant difference between microstructure of a solidified casting alloy and a solidified weld metal. According to the calculations, distribution coefficient (k) of nickel, chromium and iron is larger than 1 [10]. This leads to segregation of alloying elements into the dendrite core. In contrast, the k value of some elements such as niobium in nickels based alloys is lower than 1 and therefore this element is segregated into the interdendritic spaces. In addition, the presence of other alloying elements restricts solubility of niobium in nickel based alloys. Figure 8 shows SEM micrograph of columnar dendritic structure adjacent to the fusion line. In this area the G/R value is high and a columnar dendritic structure is formed. Ming Pang et al. have been also reported that the formation of equiaxed structure is favored when the G/R value is low enough [12].

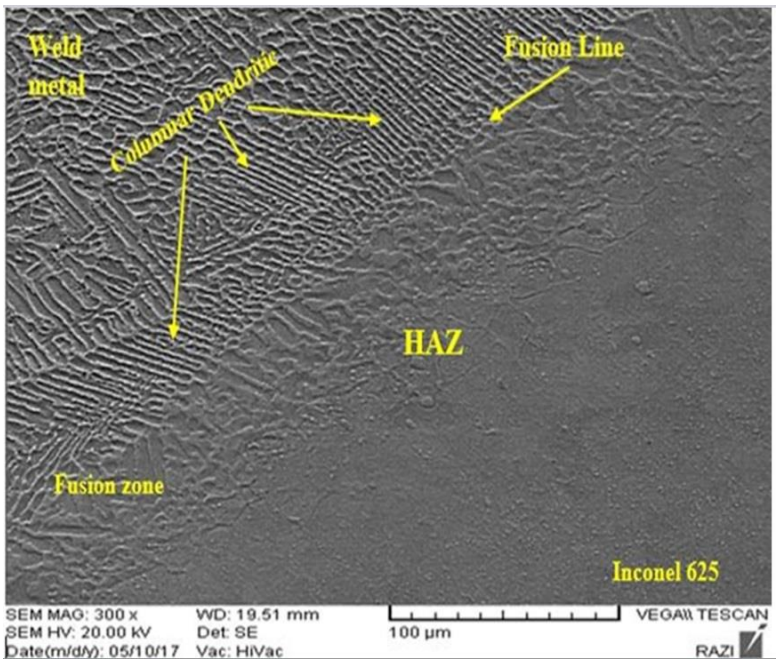

Fig. 8. SEM micrograph of the weld metal microstructure.

As shown in Fig. 9, in the center line of fusion zone, equiaxed structure is nucleated and growned and columnar dendritic structure growth is hindered. In the center line, dendritic structure is grown randomly and without any preferred crystallographic direction. Janaki et al. have been shown similar results at this area [13]. In order to show microsegregation of niobium and molybdenum during solidification of the weld metal, EDS analysis was conducted and the results are shown in Figs. 10 and 11. According to the obtained results it can be seen that the structure is rich from iron, chromium and nickel elements whereas niobium and molybdenum have been diffused from dendritic core toward interdendritic spaces. As shown in Fig. 9, it is obvious that the interdenritic spaces (which are rich from molybdenum and niobium) are lighter than dendritic cores. As discussed earlier, a composition gradient is created due to the microsegregation of niobium and molybdenum. This composition gradient causes a preferred corrosion at the dendritic cores (which are poor from molybdenum and niobium). As a result, corrosion in these areas is severe during etching process, and dendritic core would be darker.

3-2- Evaluation of mechanical properties

In order to evaluate the mechanical properties of Inconel 625/AISI 430 dissimilar laser welded joints, tensile test, microhardness measurement and fractographic analysis were performed. As mentioned above, all of the welded samples were free from any discontinuities which indicate that the laser welding processes were performed successfully.

3-2-1- Tensile properties evaluation

Tensile test results of some typical welded samples (sample A, B and C are welded with low heat input, medium heat input and high heat input, respectively) are shown in Fig. 11.

It should be noted that the tensile test was conducted normal to the welding direction. The prepared tensile test specimen was shown in Fig. 3. The mechanical properties of three typical welded samples are listed in Table 3.

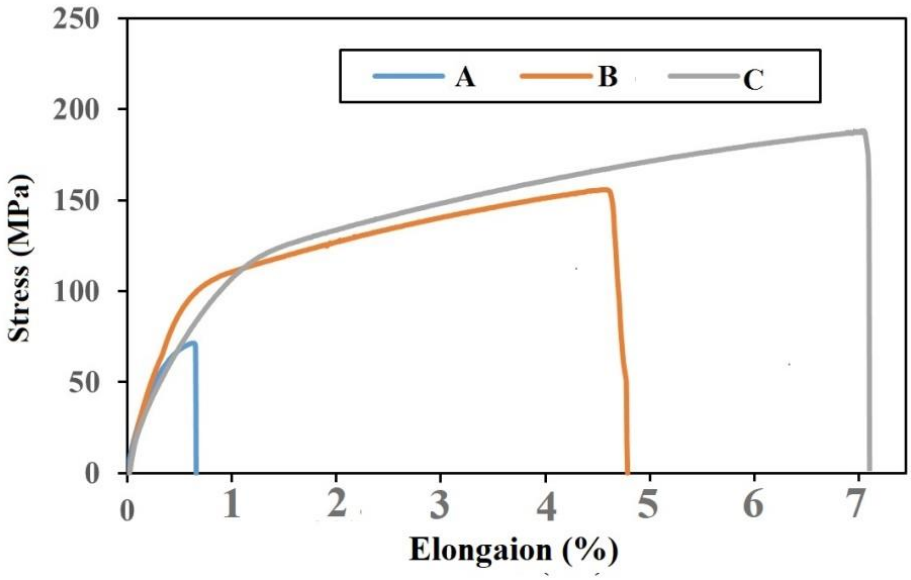

Fig. 11. Tensile test results of some typical laser welded samples.

Table 3. Elongation and tensile strength of three typical welded samples.

Specimen type	Elongation (%)	Tensile Strength (MPa)
1	0.64	**71.47**
6	4.83	**155.78**
15	7.1	**190.77**

According to the tensile test results (Fig. 11), it was found that all of the welded samples were fractured from outside of the weld metal and fracture was occurred from heat affected zone of weaker base metal i. e. AISI 430 ferritic stainless steel. This indicates a weld joint with acceptable strength which is due to the formation of fine equiaxed structure of the weld metal. It has been reported that ferritic stainless steels are usually welded at annealed condition [14]. So, some softening is expected in the heat affected zone of ferritic stainless steels due to the grain growth induced by heat delivered to the materials during laser welding. As a result, fracture is occurred from soft heat affected zone of AISI 430 ferritic stainless steel during transverse tensile test. Grain growth in heat affected zone of AISI 430 stainless steel leads to decrease in strain rate hardening and hence the strength doesn't significantly increase before fracture. This can explain fracture from heat affected zone of AISI 430 ferritic stainless steel [15-17].

Regarding presence of various regions with different properties and deformation behaviors in dissimilar weld joints, interpretation of fracture mechanism in these joints is more complex than that of similar weld joints. In other words, deformation in a soft region adjacent to a harder region may lead to fracture from other regions.

As can be seen from the tensile test results, the welded samples have a continuous yield features and don't show a yield point. Softening of heat affected zone due to the grain growth is harmful for deformation of laser welded components. Fracture form heat affected zone is also confirmed by scanning electron and optical microscopy. Grain growth in heat affected zone leads to decrease in density of grain boundaries in this region in contrast to the weld metal and even base metal. In regions with large grain size dislocations movement is faster and easier and hence deformation is concentrated in this region. In other words, the majority of plastic deformation in tensile test is taking place in regions in which dislocations are less pinned [18]. A fractured tensile test specimen is shown in Fig. 12.

3-2-2- Fractography

Studying the fracture surface is a valuable method for analyzing the fracture of welded components. For this purpose, fracture surface of three typical welded samples (i. e. a samples welded with low, medium and high heat inputs) were analyzed by SEM. As discussed earlier, fracture was occurred from heat affected zone of AISI 430 stainless steel. The fracture surfaces of different laser welded samples are shown in Figs. 13-15. The presence of dimples in the fracture surface indicates ductile fracture of laser welded samples. The coarse dimples in the fracture surfaces are indications of completely ductile fracture [19, 20]. The only difference between the tensile characteristic of laser welded samples is variation in their fracture energies and also the depth of each dimples observed in the fracture surfaces. Very small area in the fracture surface of low heat input sample has brittle fracture features. This can be due to the presence of some porosity in the weld line which is formed due to the instability of laser beam. The sample with greatest dimple depth is a sample with highest heat input (See Fig. 15). Since deep dimples are indications from ductile samples, thus the sample with highest heat input has higher elongation in comparison to other welded samples. Also, the dimple size has an inverse relation to the strength of materials. So, the smaller dimple size leads to higher strength [21].

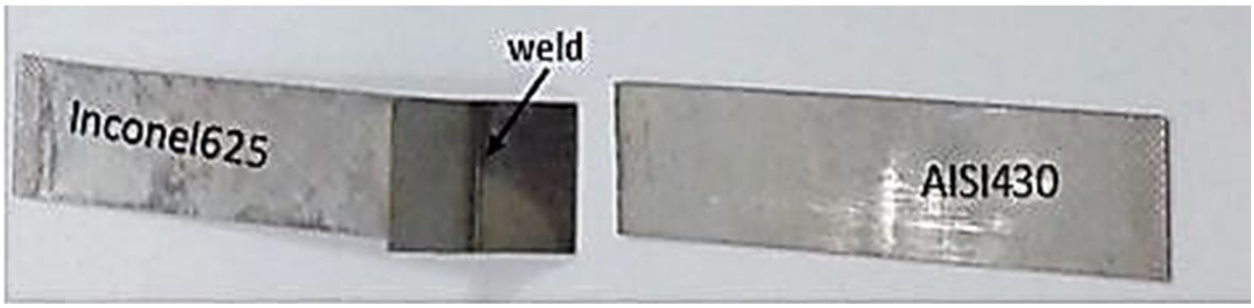

Fig. 12. A typical fractured tensile test specimen.

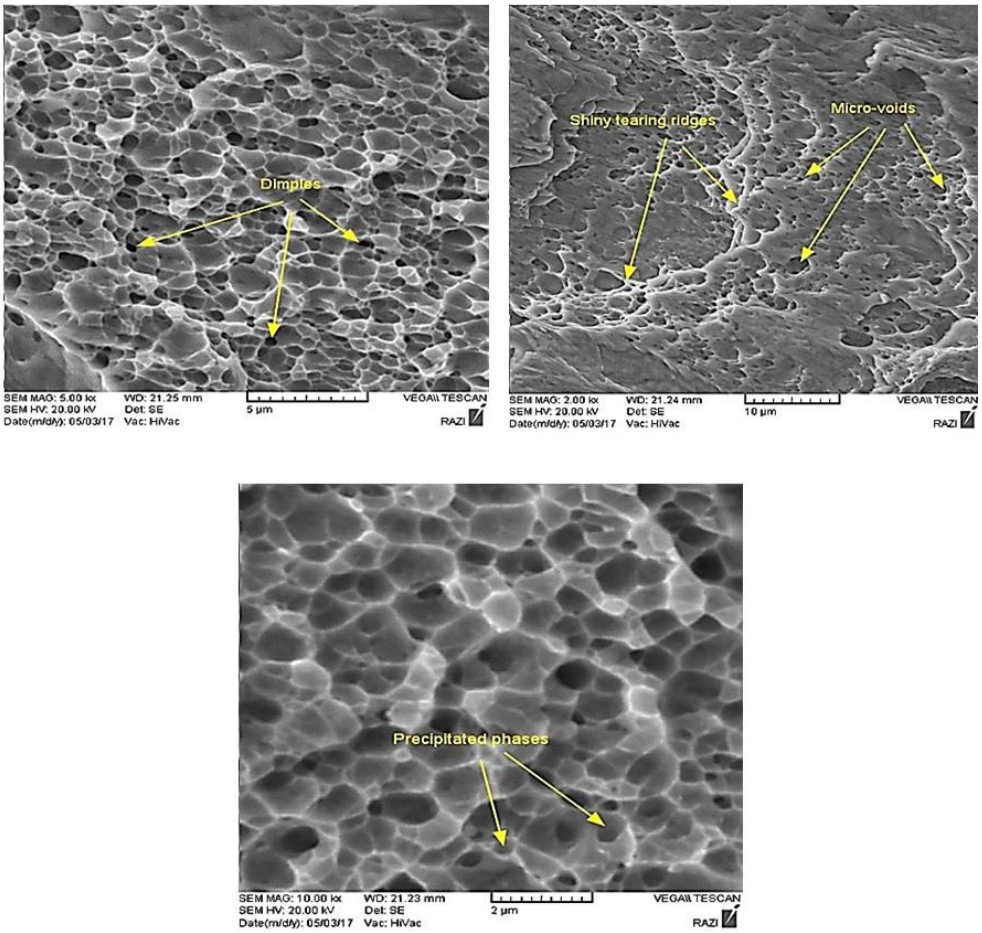

Fig. 13. Fracture surface of the laser welded sample with low heat input.

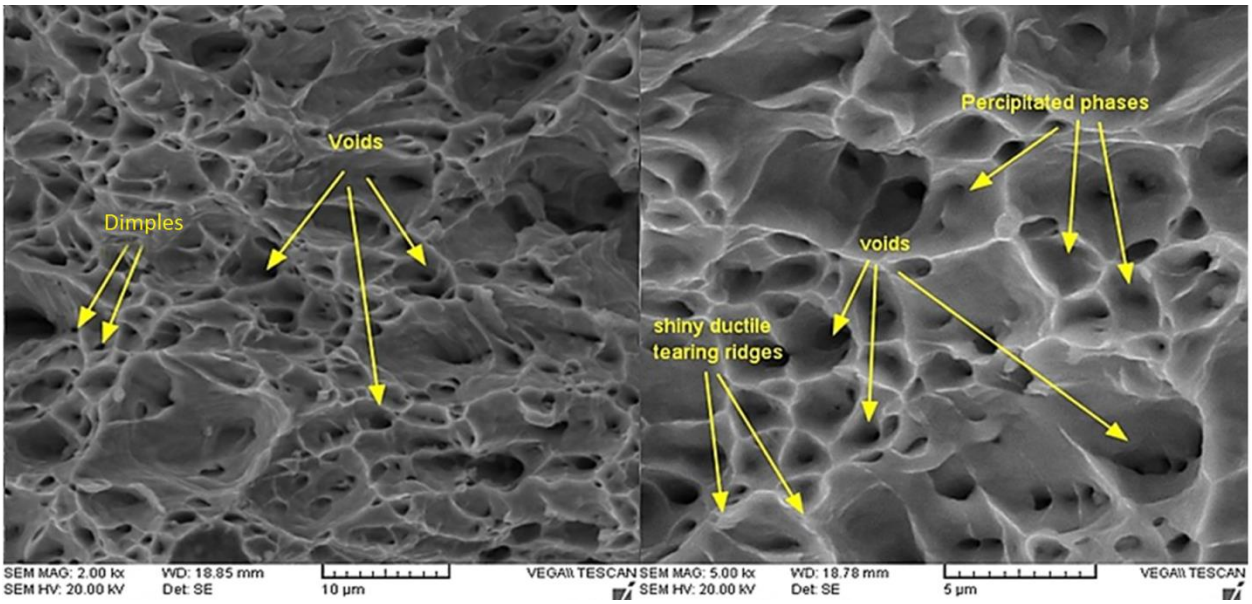

Fig. 14. Fracture surface of the laser welded sample with high heat input.

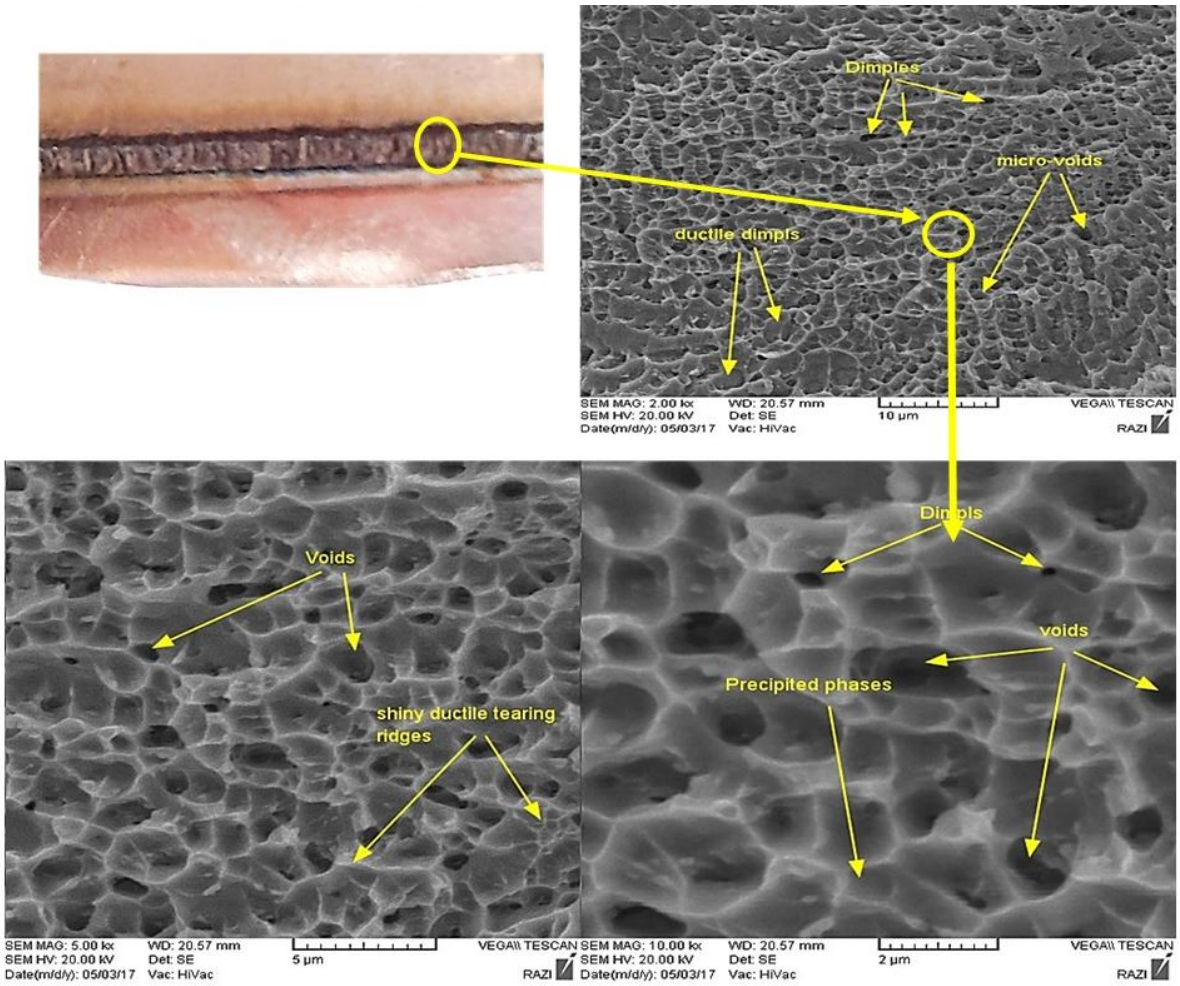

Fig. 15. Fracture surface of the laser welded sample with medium heat input.

3-2-3- Microhardness measurement

In order to investigate the hardness of various zones of the welded joints, Vickers microhardness was done on the overall cross section of the joints from one base metal to another. Microhardness profile is an appropriate criterion which confirms the formed microstructures at various zones. Figure 16 shows the microhardness profiles of two welded samples (a welded sample with a high input (A) and a sample with a low heat input (B)). For each zone, microhardness measurements were taken from three points at an interval of four times the indenter size to avoid the effects of localized strain hardening in vicinity of the indentation. Finally, the averages of the three measurements were reported. Generally, an increasing trend in the hardness value can be observed from AISI 430 ferritic stainless steel base metal toward Inconel 625 base metal. It is well-known that nickel based superalloys have higher hardness than that of metals with fully ferritic structures. As shown in Fig. 16, the average hardness at the weld metal across the center line is higher than that of AISI 430 base metal and lower than that of Inconel 625. This can be attributed to the formation of different phase and microstructure in this area.

Diffusion of solvent elements i. e. niobium and molybdenum from the lattice solid solution and microsegregation of them is the main reason responsible for decrease in hardness of the weld metal [17, 20]. In addition, the hardness of the weld metal in vicinity of Inconel 625 is higher than that of vicinity of AISI 430. This can be related to the formation of higher fraction of chromium carbide and also a stronger solid solution due to the higher concentration of chromium in the Inconel 625. The lower hardness in heat affected zones is also because of the grain growth in these areas [16].

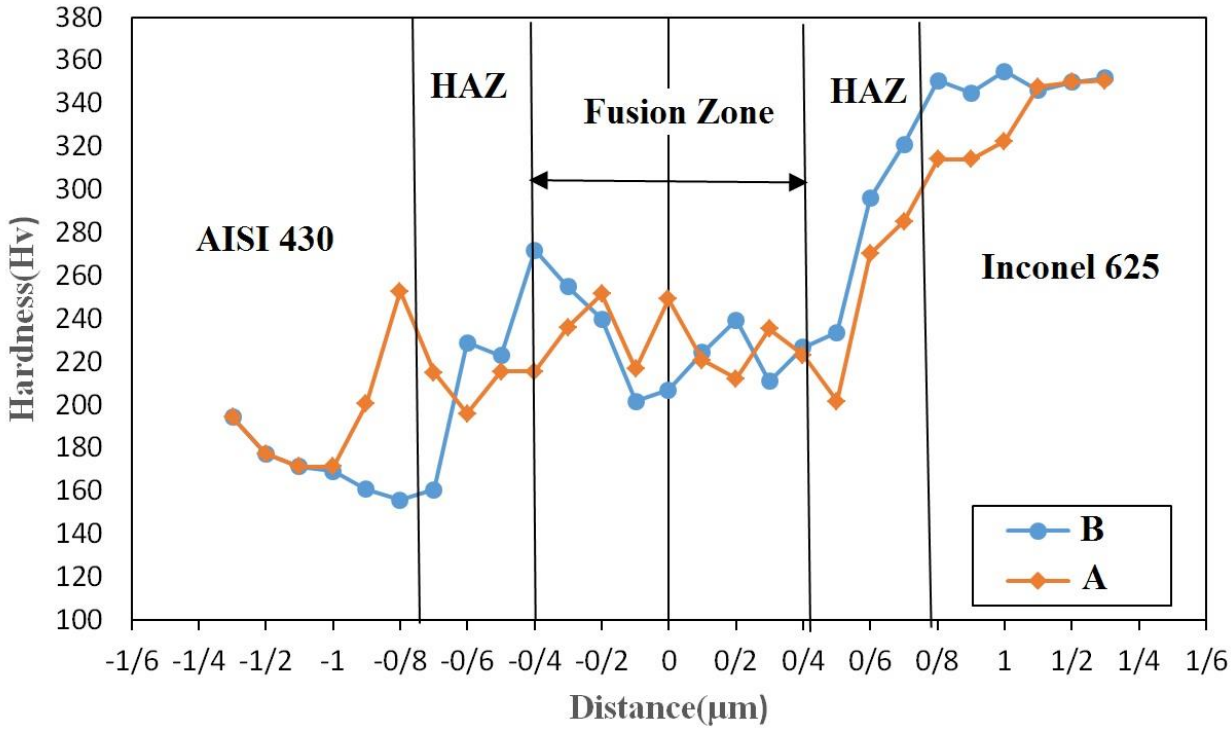

Fig. 16. Microhardness profiles of two typical samples.

3-3- Optimization of tensile strength

It was mentioned earlier that all of the laser welded samples were fractured form the heat affected zone of AISI 430 ferritic stainless steel. This was due to the grain coarsening with lower hardness of this area. Regarding to the complexity of laser welding process in choosing proper parameters values, achieving the maximum tensile strengths of the weld joint via a more accurate study based on the mathematical modeling is of prime importance. The complexity of this process arise from significant changes (which are usually undesirable) in weld bead geometry, weld metal microstructure, residual stress and… due to the little changes in parameters values. For this purpose, this section is discussed about the optimization of the process parameters in order to obtain the maximum tensile strength by means of response surface methodology. Hence a theoretical model will be proposed which make a correlation between the process parameters and tensile strength. According to the correlation between mechanical properties and microstructural features, any factors that influence temperature conditions (temperature gradient, peak temperature and temperature distribution), cooling rate and weld bead geometry, can considerably affect properties of the weld joints. It has been shown by other researchers that three factors i. e. lamping current, pulse duration and travel speed have significant effect on the mechanical properties of laser welded components [22-24]. Thus, these parameters were considered as the main effective factors. After determining the main process parameters, the working limit of each parameter was appointed based on experimental efforts and literatures. In order to find the range of each selected parameter, trial experiments were performed by changing one parameter at a time, while keeping other process parameters at a constant setting. The weld bead appearance and weld soundness were inspected to identify the working limits of the welding parameters. The absence of macro defects with uniform, flat and smooth welded surface and the sound face were the criteria for choosing the conceivable and feasible working range.

In order to conduct response surface methodology, three levels of each parameters were considered. A mathematical model developed based on regression was used to predict relation between welding parameters and tensile strength of each weld joint. Thus:

$$\sigma_{UTS} = f(I, T_p, S,) \quad (4)$$

Thus, the second order polynomial (regression) equation was used to represent the response surface σ_{UTS} is:

$$\sigma_{UTS} = b_\circ + \sum_{i=1}^{k} b_i x_i + \sum_{i=1}^{k} b_{ii} x_i^2 + \sum_{i<j} \sum_{j=2}^{k} b_{ij} x_i x_j + \varepsilon \quad (5)$$

Where $b_{\circ}$ is the response of the central point, the coefficient b_i is linear terms, the coefficient b_{ii} is the quadratic terms and the coefficient b_{ij} refers to the interaction terms [25-27].

All the co-efficient were calculated for their significance at 95% confidence level. Accordingly, when the calculated value of P corresponding to a coefficient exceeds the standard tabulated value for the desired level of confidence (say 5%), the coefficient becomes insignificant. The significant regression coefficients were recalculated and the final models were developed using only these significant coefficients.

Design of experiment matrix and the order of the test are also shown in Table 4.

The results of variance analysis (ANOVA) are given in Table 5.

Table 4. Design of experiment matrix.

Exp. No.	Factors		
	Lamping current	**Travel speed**	**Pulse duration**
1	**-1**	**-1**	**-1**
2	**1**	**-1**	**-1**
3	**-1**	**1**	**-1**
4	**1**	**1**	**-1**
5	**-1**	**-1**	**1**
6	**1**	**-1**	**1**
7	**-1**	**1**	**1**
8	**1**	**1**	**1**
9	**-1**	**0**	**0**
10	**1**	**0**	**0**
11	**0**	**-1**	**0**
12	**0**	**1**	**0**
13	**0**	**0**	**-1**
14	**0**	**0**	**1**
15	**0**	**0**	**0**
16	**0**	**0**	**0**
17	**0**	**0**	**0**
18	**0**	**0**	**0**
19	**0**	**0**	**0**
20	**0**	**0**	**0**

Table 5. ANOVA results for tensile strength response.

Term	**Coef.**	**SE Coef.**	**T**	**P**
Constant	189433	1.815	104.355	0.000
I	38.415	1.670	23.006	0.000
S	-0.658	1.670	-0.394	0.702
T_P	12.597	1.670	7.544	0.000
I×I	-35.115	3.184	-11.028	0.000
S×S	-5.380	3.184	-1.690	0.122
T_P×T_P	-15.955	3.184	-5.011	0.001
I×S	11.780	1.867	6.310	0.000
I×TP	-19.260	1.867	-10.317	0.000
S×T_P	-1.063	1.867	-0.569	0.582

According to the resulted ANOVA, after determination of the significant coefficients, mathematical model was developed by using these coefficients only after the elimination of the insignificant coefficients. The mathematical model in terms of coded factors is shown below:

$$\sigma_{UTS} = 189433 + 38.415I + 12.597T_p - 35.115I^2 - 15.955T_p^2 + 11.780I \times S - 19.260I \times T_p \quad (6)$$

The validity of the above-mentioned mathematical model was evaluated using the ANOVA. ANOVA test results for the developed model are presented in Table 6. The results of the ANOVA showed that the regression is significant with linear, quadratic and interaction terms for the developed model.

The accuracy of the model was checked by residual plots for σ_{UTS} as shown in Fig. 17.

The normal probability plot of the residuals for σ_{UTS}, as shown in this figure, revealed that the residuals are falling on the straight line, indicating that the errors are distributed normally. The coefficient of determination, 'R^2', is used to find how close the predicted and experimental values are [25]. The value of 'R^2' for the above-developed relationship is also listed in Table 6. It shows a high correlation between the experimental values and the predicted values. The 'Pred R^2' of 99.16% is in a reasonable agreement with the 'Adj R^2' of 94.12%. All above considerations indicate the adequacy of the developed relationship. At final step, the main effect of each significant parameter was analyzed. Figure 18 shows the main effect plot of the selected factors on the tensile strength of the weld joints. It can be observed that there is a convenience relationship between each parameters and tensile strength. It can be concluded from the slope of each curve that the pulse duration and lamping current have more significant effect on the tensile strength. In other words, travel speed is a less effective factor.

Table 6. ANOVA test results for checking adequacy of the proposed model.

Source	DF	Seq SS*	Adj SS†	Adj MS‡	F	P	Significance
Regression	9	33208.6	33028.6	3669.8	131.62	0.000	√
Linear	3	16348.3	16348.3	5449.4	195.44	0.000	√
I (A)	1	14757.1	14757.1	14757.1	529.26	0.000	√
S (mm.min)	1	4.3	4.3	4.3	0.16	0.702	
T_p (mms)	1	1586.8	1586.8	1586.8	56.91	0.000	√
Square	3	12593.5	12593.5	4197.8	150.55	0.000	√
I×I	1	11480.2	3391.0	3391.0	121.62	0.000	√
S×S	1	413.2	79.6	79.6	2.86	0.122	
T_P×T_P	1	700.1	700.1	700.1	25.11	0.001	√
Interaction	3	4086.8	4086.8	1362.3	48.86	0.000	√
I×S	1	1110.1	1110.1	1110.1	39.82	0.000	√
I×T_P	1	2967.6	2967.6	2967.6	106.43	0.000	√
S×T_P	1	9.0	9.0	9.0	0.32	0.582	
Residual Error	10	278.8	27.9				
Lack-of-Fit	5	234.8	234.8	47.0	5.33	0.045	√
Pure Error	5	44.0	44.0	8.8			
Total	19	33307.4					

R^2 = 99.16% , Pred R^2 = 94.12% , Adj R^2 = 98.41

* Sum of Square

† Mean Square

‡ Degree Freedom

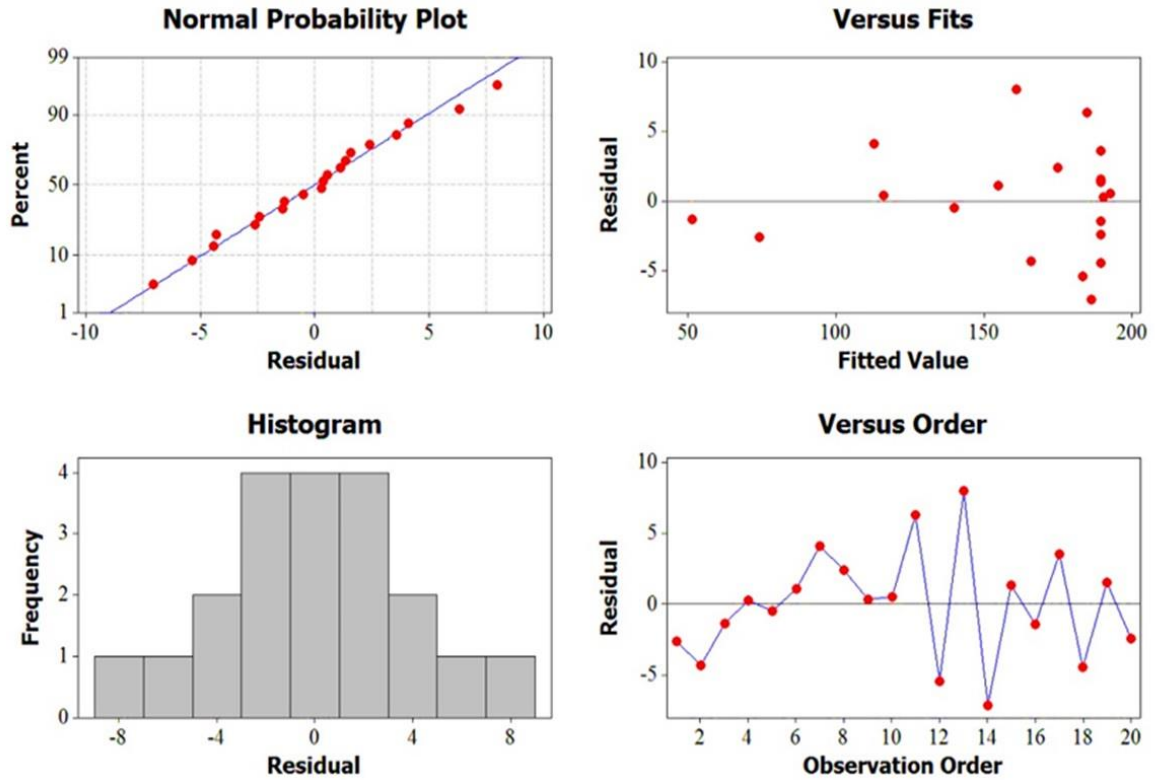

Fig. 17. Normal probability plots of tensile strength response.

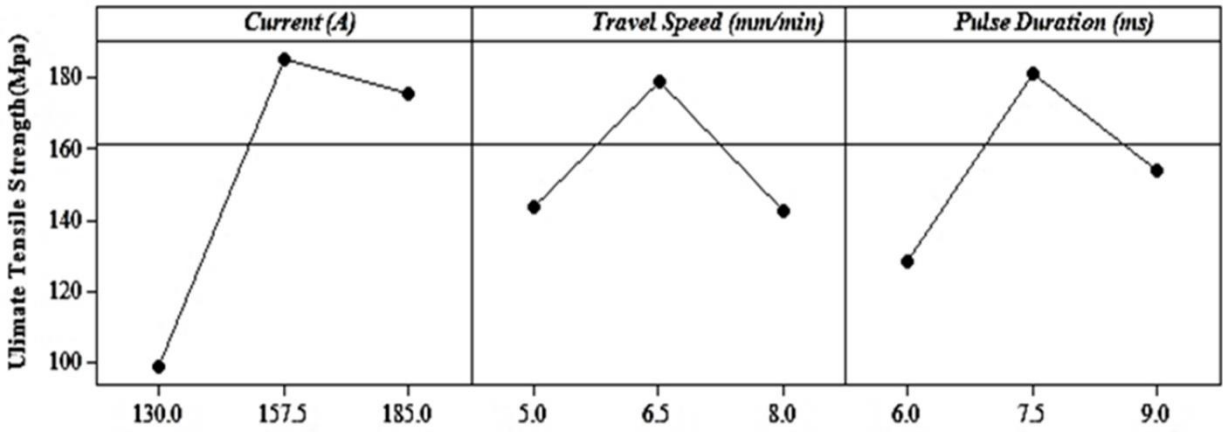

Fig. 18. Plots of main effects on the tensile strength response.

By using counter plots and 3D response graph, it would be capable to describe the effect of each process parameter. If a contour patterning of circular shaped contours occurs, this means the independence of factor effects, while elliptical contours may suggest factor interactions [25]. The interaction effect of the lamping current and the pulse duration on the tensile strength of the weld joints is shown in Fig. 19 using 3D response graph and counter plot. It can be clearly concluded that by increasing in pulse duration, tensile strength increases up to a maximum value and then decreases by further increase in pulse duration.

When the pulse duration is low, the heat input is not sufficient to produce a cohesive, coalescent and continuous weld joint. Also at low heat input the penetration is not complete. By increasing in pulse duration, a coalescent joint with full penetration is achieved which shows a high tensile strength. By further increase in pulse duration, due to the low heat conductivity, enlargement of grains in heat affected zone is significant and thus a decrease in tensile strength is expected. As can be seen from this figure, the maximum tensile strength is achievable when the lamping current is between 150 to 180 A.

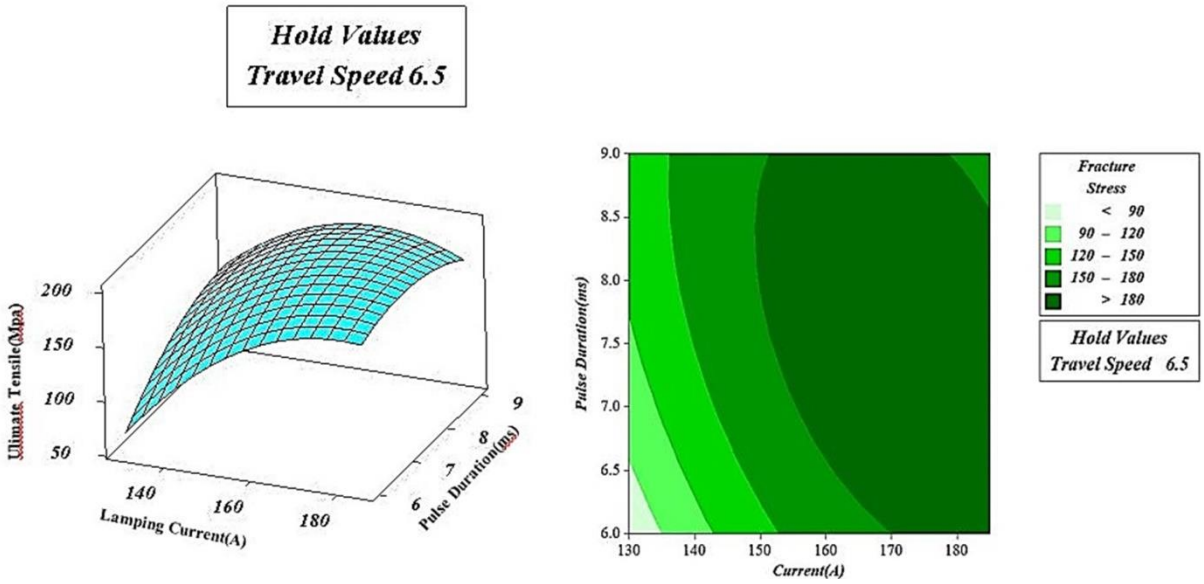

Fig. 19. Interaction effect of lamping current and pulse duration on tensile strength value of the welded samples.

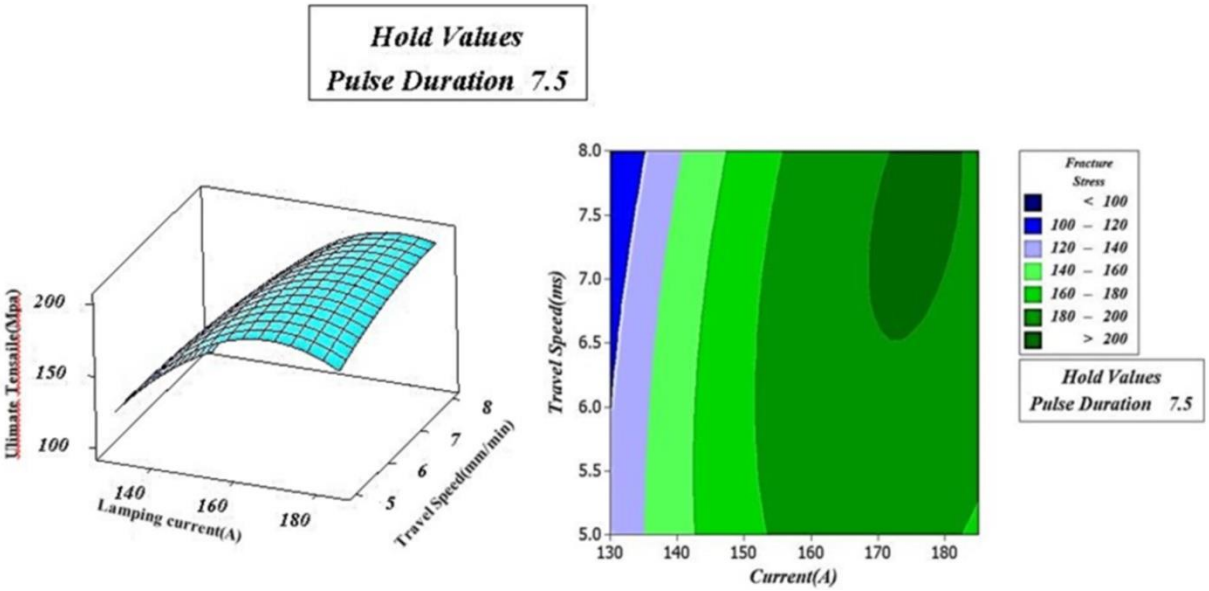

Fig. 20. Interaction effect of lamping current and travel speed on tensile strength value of the welded samples.

Counter plot and response graph showing the interaction effect of lamping current and travel speed is presented in Fig. 20. As can be seen, the tensile strengths of the weld joints are decreased by decreasing in lamping current and increase in travel speed. Increase in travel speed causes decrease in heat input and thus a joint with lack of penetration is produced. In other words, a maximum tensile strength is obtained when a complete coalescence and full penetration between two base metals is generated. Decrease in tensile strength at very high lamping current and very low travel speed is due to the excessive heat input which causes grain coarsening and therefore decreases in tensile strength.

4- Conclusions

1- Solidification mode in center line of the weld metal was completely very fine equiaxed structure, whereas the structure in fusion line was columnar dendritic structures which were competitively grown in different direction.

2- The majority of formed carbides in the weld metal were niobium-rich carbides. Dendritic structure of solidified weld metal is accomplished with accumulation of nickel and

iron at the dendritic cores and microsegregation of niobium and molybdenum to the interdenritic spaces.

3- The heat affected zone was very narrow in the samples with maximum tensile strength, while the welded sample with high heat input had a wide heat affected zone with larger grain size.

4- The hardness profiles showed an increasing trend form AISI 430 base metal to the Inconel 625 base metal.

5- The five-level factorial technique could be employed easily for developing mathematical models used in predicting the tensile strength values of the welded samples within the workable region of the control parameters in dissimilar laser welding of Inconel 625/AISI 430 joint.

6-The ANOVA demonstrated that the lamping current was the most significant factor affecting the tensile strength value. In addition, the travel speed had a less effect on the responses.

References

[1] Cai D, Nie P, Shan J, LiuW, Gao Y, YaoM(2006) Precipitation and residual stress relaxation kinetics in shot-peened Inconel 718. J Mater Eng Perform 15(5):614–617

[2] Mathew MD, Parameswaran P, Rao KBS (2008) Microstructural changes in alloy 625 during high temperature creep.Mater Charact 59(5):508–513

[3] J.C. Lippold, D.J. Kotecki, Welding metallurgy and weldability of stainless steels. New Jersey, Wiley- Interscience, 2005.

[4] Silva CC, de Miranda HC, Motta MF, Farias JP, Afonso MCR, Ramirez AJ (2013) New insight on the solidification path of an alloy 625 weld overlay. J Mater Res Technol 32:1–10.

[5] Shankar V, Rao SKB, Mannan SL (2001) Microstructure and mechanical properties of Inconel 625 superalloy. J Nucl Mater 288: 222–232

[6[Kuo CP, Ling CC, Chen SH, Chang CW (2005) The prediction of cutting force in milling Inconel-718. Int J Adv Manuf Technol 27: 655–660

[7] K.Devendraneth Ramkumar,Aditya Chandrasekhar,N.Arivazhagan" Investigations on Structure – property Relation ships of Inconel 718 and AISI430 Dissimilar Weld ments "Metalloger . microstrruct .anal .DOI 10.1007/s13632-015- 02008 - 2.2015

[8] Huang Q, Hagstroem J, Skoog H, Kullberg G (2009) Effect of laser parameter variation on sheet metal welding. Int J Join Mater 3(1991):79–88

[9] S. Zhou, D. Chai, Jingling Yu, G. Ma, Dongjiang Wu," Microstructure characteristic and Mechanical Property of pulsed laser lap-welded nickel-based superalloy and stainless steel", Journal of Manufacturing Processes Vol. 25, pp.220 –226 , 2017.

[10] S.Kou,welding metallurgy , second ed.Hoboken, Jon Wily & Sons Inc,2003

[11] W.C.Winegard, am introduction to the solidification of metal. Institute of Metals,1994.

[12] Ming ,pang , Gang Yu,Heng.hai wang, Cai-Yan Zheng," Microstructure Study of Laser Welding Cast Nikel-Based Superahhoy K418", Jornal of Materials Poroccessing Technology ,Vol.207, pp.271-275, 2008.

[13] G.D.Janaki Ram, A.Venugopal Reddy, K.Prasad Rao," Microstructur and tensile propertis of Inconel 718 pulsed Nd-YAG laser welding ", journal of matrials Poroccessing Technology, No. 167, pp. 73-82, 2005.

[14] N.Sheik Thavudu, S.Kamatchisankaran S.Roseline Dr.S.Guharaja "An Experimental Investigation and Evaluation of SS430 Using Nd- YAG Laser Welding Process" Vol. 5, 2016.

[15] Nikhil Kumar,n, ManidiptoMukherjee, AsishBandyopadhyay" Comparative study of pulsed Nd:YAG laser welding of AISI 304 and AISI 316 stainless steels" , Optics &LaserTechnology Vol. 88 , PP. 24–39, 2017

[16] ASM Handbook," Properties and Selection:Irons, Steels, an High Performance Alloys",ASM International, Materials Park, Ohio,Vo. l.1, 2002

[17] Li,Gang . Hang,J . W,Yixiong , " An investigation on microstructure and properties dissimilar welded Inconel 625 and SUS 304 using high – power CO2 Laser", int j adv Manuf Technol, No. 76, pp. 1203-1214, 2015.

[18] H. Shah Hosseini, M. Shamanian &A. Kermanpur, "Characterization ofMicrostructures and MechanicalProperties ofInconel 617/310 Stainless Steel DissimilarWelds", Materials Characterization, Vol. 62, pp. 425-431, 2011.

[19] Theriault A, Xue L, Dryden JR (2009) Fatigue behavior of laser consolidated IN-625 at room and elevated temperatures. Mater Sci Eng A 516:217–225

[20] K. Devendranath Ramkumara, Winston Sunny Abrahama, Vedha Viyasha, N. Arivazhagana, Arul Maximus Rabelb Investigations on the microstructure, tensile strength and high temperature corrosion

behaviour of Inconel 625 and Inconel 718 dissimilar joints, Journal of Manufacturing Processes 25 (2017) 306–322.
[21] Hertzberg, R.W., Deformation and Fracture Mechanics of Engineering Materials, 4th Edition, John Wiley & Sons, USA, 1995.
[22] Y.G. Song, W.S. Li, L. Li, Y.F. Zheng, The influence of laser welding parameters on the microstructure and mechanical property of the as-jointed NiTi alloy wires, Mat. Lett. 62 (2008) 2325-2328.
[23] M. Hazratinezhad, N.B. Mostafa Arab, A.R. Sufizadeh, M.J. Torkamany, Mechanical and metallurgical properties of pulsed neodymium-doped yttrium aluminum garnet laser welding of dual phase steels, Mater. Design. 33 (2012) 83-87.
[24] F. Malek Ghaini, M.J. Hamedi, M.J. Torkamany, J. Sabbaghzadeh, Weld metal microstructural characteristics in pulsed Nd: YAG laser welding, Scripta. Mater. 56 (2007) 955-958.
[25] D.C. Montgomery, Design and Analysis of Experiments, 2nd ed., John Wiley
and Sons, New York, 1984
[26] Miller I, Freund JE, Johnson d RA. Probability and statistics for engineers. 5nd
ed. New Delhi: Prentice of Hall of India, Pvt. Ltd; 1999.
[27] Egbewande AT, Buckson RA, Ojo OA (2010) Analysis of laser beam weldability of Inconel 738 superalloy. Mater Charact 61: 569–574